Increasing understanding and confidence in THM simulations of Engineered Barrier Systems

Annika Schäfers Dr.-Ing.
Federal Institute for Geosciences and Natural Resources, Hanover, Germany (corresponding author: annika.schaefers@bgr.de)

Antonio Gens PhD
Universitat Politècnica de Catalunya, Barcelona, Spain

Alfonso Rodriguez-Dono PhD
Universitat Politècnica de Catalunya, Barcelona, Spain; Institute of Environmental Assessment and Water Research (IDAEA), Spanish National Research Council (CSIC), Barcelona, Spain

Steven Baxter PhD
Wood, Didcot, UK

Vasileios Tsitsopoulos PhD
Wood, Didcot, UK

David Holton PhD
Wood, Didcot, UK

Daniel Malmberg PhD
Clay Technology, Lund, Sweden

Masataka Sawada DrEng
Central Research Institute of Electric Power Industry, Abiko, Japan

Qiao Yafei PhD
Department of Geotechnical Engineering, Civil Engineering College, Tongji Univeristy, Shanghai, China

Alessio Ferrari PhD
École Polytechnique Fédérale de Lausanne, Lausanne, Switzerland; Università degli Studi di Palermo, Palermo, Italy

Lyesse Laloui PhD
École Polytechnique Fédérale de Lausanne, Lausanne, Switzerland

Anders Sjöland PhD
Swedish Nuclear Fuel and Waste Management Company, Stockholm, Sweden

Previous studies on the modelling of coupled thermo-hydro-mechanical (THM) processes in bentonite-based engineered barrier systems (EBSs) showed the sensitivity of the output quantities to changes in the input parameters. To investigate the effects of uncertainties on the modelling results, to improve the understanding of the coupled processes active in the repository near field and to gain in-depth understanding of model uncertainties of different codes, a sensitivity analysis and code comparison of EBS simulations was performed within the Task Force on Engineered Barrier Systems. The analysis included variations in material parameter values, boundary and initial conditions, considered physical processes and model geometries, amounting to 60 different cases. This in-depth analysis helped evaluate the influence of parameter and conceptual uncertainties on the results of coupled THM simulations and to identify key parameters and processes. The cross-code comparison encouraged a fruitful exchange among modelling teams and led to very good agreements between the results of the different codes. Serving as a benchmark example for THM-coupled simulations of bentonite-based EBSs, the study helped increase the confidence in the modelling capabilities of several codes used for safety evaluations of repositories for spent fuel and high-level radioactive waste.

Notation

a_i	fuel age coefficients
c	specific heat capacity (J/(kg K))
$\boldsymbol{D}$	elasticity tensor
$\mathrm{d}\boldsymbol{\varepsilon}_\mathrm{T}$	strain increment due to temperature changes
E	Young's modulus (MPa)
$\mathbf{I}$	unity matrix
k_i	intrinsic permeability (m^2)
k_rel	relative permeability
m_R	parameter of the van Genuchten function
n	porosity
P	canister power (W)
P_0	parameter of the van Genuchten function (MPa)
p_l	pore pressure (MPa)
q_h	heat flux ($\mathrm{W/m}^2$)
q_l	liquid phase flux (m/s)
S_l	liquid saturation
s	suction (MPa)
T	temperature (K)
t	time (years)
t_i	time constants (years)
$\boldsymbol{u}$	displacement (m)
X	independent variable
Y	dependent variable
α_T	thermal expansion coefficient (K^{-1})
β	effective stress parameter
δ	parameter of the relative permeability function
$\boldsymbol{\varepsilon}$	strain
ε_hs	hygroscopic strain
λ	heat conductivity (W/(m K))
μ	viscosity (Pa s)
ρ	density ($\mathrm{kg/m}^3$)
$\boldsymbol{\sigma}$	total stress (MPa)
$\boldsymbol{\sigma}'$	effective stress (MPa)
σ_rad, σ_tan, σ_axi	radial, tangential and axial stress components (MPa)
$\sigma_\mathrm{sw,max}$	maximum swelling pressure at a change of liquid saturation of $\Delta S_\mathrm{l} = 1{\cdot}0$ (MPa)
τ	tortuosity
υ	Poisson' ratio
χ	Bishop's parameter

Introduction

In many concepts for the deposition of high-level nuclear waste, clay-rich materials are intended as an engineered barrier between the waste canister and the surrounding host rock. The behaviour of these materials is characterised by their swelling properties and low hydraulic conductivity, which makes a clay-rich material a favourable component of a multiple-barrier system to limit contaminant transport from the waste canisters. The heat-emitting canister, together with the geological and the geotechnical barriers, is the seat of a system of strongly coupled thermal, hydraulic, mechanical and chemical (THM-C) processes. The ability to understand these interacting processes and to represent them in numerical models is essential for safety evaluations of repositories for spent fuel and high-level radioactive waste.

Previous studies on the thermo-hydro-mechanical (THM) modelling of engineered barrier systems (EBSs) showed the sensitivity of important output quantities to changes in the input parameters (Gens *et al*., 1998; Rutqvist and Tsang, 2008). To investigate the effects of uncertainties on the modelling results, to improve the understanding of the coupled processes active in the repository near field and to gain in-depth understanding of model uncertainties of different numerical codes, a sensitivity analysis and code comparison of EBS simulations was chosen as one of the tasks within the project Task Force on Engineered Barrier Systems. Initiated in 2004 by the Swedish Nuclear Fuel and Waste Management Company (SKB), the project's objectives are to verify and enhance the capability to model the coupled THM-C processes in bentonite buffers and the repository near field. This paper describes the main outcomes of the sensitivity analysis and the code comparison performed within the Task Force on Engineered Barrier Systems.

The base case model of the sensitivity analysis and the code comparison is not only a simplified, but also a meaningful representation of a single deposition hole in the Swedish disposal concept KBS-3V. The sensitivity analysis is not a site-specific task. To obtain a representative base case model and relevant parameter ranges, it was necessary to define thoroughly the material parameters based on literature data of experimental findings from representative sites and samples. The sensitivity analysis included variations of material parameter values, boundary and initial conditions, considered physical processes and alternative model geometries, amounting to 60 different modelling cases. This in-depth analysis helped evaluate the influence of parameter and conceptual uncertainties on the results of coupled THM modelling of EBS and identify key parameters and key processes.

A subtask of the sensitivity analysis was code comparison, using the base case model of the sensitivity analysis as a reference case. The code comparison was divided into the following stages with increasing complexity

(*a*) stage 1: thermo-hydraulic (TH) calculation neglecting vapour diffusion
(*b*) stage 2: TH calculation considering vapour diffusion
  (*i*) stage 2a: with constant fluid properties
  (*ii*) stage 2b: with temperature-dependent fluid properties
  (*iii*) stage 2c: using a two-phase flow approach
(*c*) stage 3: THM calculation
  (*i*) stage 3a: with only elastic material behaviour
  (*ii*) stage 3b: with an additional simplified swelling term for the bentonite.

Six teams participated in the subtask, providing results of six different numerical codes (Wood using Tough2–Flac3D, the Federal Institute for Geosciences and Natural Resources (BGR) using OpenGeoSys (OGS), Clay Technology using Comsol, the Central Research Institute of Electric Power Industry (Criepi) using Lostuf, École Polytechnique Fédérale de Lausanne (EPFL) using Lagamine and Universitat Politècnica de Catalunya (UPC) using Code_Bright). The results were compared in terms of evolution of temperature, pore pressure, saturation and stress components.

Task description

Base case description

Geometry

Based on the Swedish disposal concept for spent nuclear fuel, the base case model of the sensitivity analysis and the code comparison is a simplified representation of a single KBS-3V deposition hole in a two-dimensional (2D) axisymmetric model (Figure 1). The different bentonite elements are simplified to a homogeneous buffer material. The access tunnel and backfill material are neglected. To reduce the mesh size, the canister is not discretised; instead, the heat source term is applied to the canister–buffer interface. To study the influence of geometric model simplification, models with the bentonite blocks, rings and pellets as materials with different initial properties were part of the assessment modelling.

Considered physical processes

In the base case, the coupled TH processes are considered, applying Richards's approximation in order to reduce the complexity of the models. The gas phase pressure is assumed to be at atmospheric pressure at any time. Vapour diffusion, temperature-dependent fluid properties and a two-phase flow simulation are considered in specific cases of the code comparison and sensitivity analysis.

The mechanical behaviour of the rock is simulated by an elastic material law. For the buffer, a simplified swelling law was proposed in the task description in order to facilitate the comparison and to allow for a relatively easy implementation. It defines the build-up of swelling pressure proportional to the change in liquid saturation. The effective stress increment is calculated by

$$1.\quad \mathrm{d}\boldsymbol{\sigma}' = \boldsymbol{D}:(\mathrm{d}\boldsymbol{\varepsilon} - \mathrm{d}\boldsymbol{\varepsilon}_{\mathrm{T}}) - \Delta S_{\mathrm{l}}\sigma_{\mathrm{sw,max}}\mathbf{I}$$

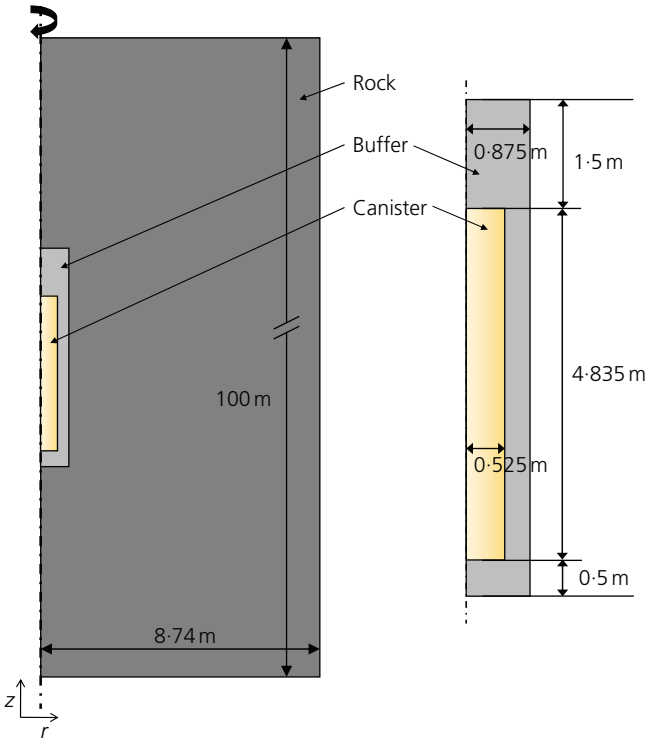

Figure 1. Model dimensions

where $\boldsymbol{D}$ is the elasticity tensor; $d\boldsymbol{\varepsilon}$ is the elastic strain increment; $d\boldsymbol{\varepsilon}_T$ is the strain increment due to temperature changes; S_l is the liquid saturation; and $\mathbf{I}$ is the unity matrix. The model parameter $\sigma_{sw,max}$ corresponds to the maximum swelling pressure at a change of liquid saturation of $\Delta S_l = 1{\cdot}0$.

The total stress is defined according to Equation 2.

$$\boldsymbol{\sigma} = \boldsymbol{\sigma}' - \chi\beta p_l \mathbf{I} \quad (2)$$

Here, compression stress is negative, while pore pressure p_l is positive. The effective stress formulation is chosen that is available to all codes applied in the comparison; with the effective stress parameter $\beta = 1{\cdot}0$ and Bishop's parameter χ being defined as follows

$$\chi = \begin{cases} 0{\cdot}0 \text{ if } S_l < 1{\cdot}0 \\ 1{\cdot}0 \text{ if } S_l = 1{\cdot}0 \end{cases} \quad (3)$$

Boundary and initial conditions

The calculation sequence is divided into two phases – a purely hydraulic calculation of the open deposition hole followed by a TH or THM calculation of the time after disposal of the waste canister. The boundary and initial conditions applied to the benchmark model are summarised in Figure 2.

In the first phase, atmospheric pressure is applied to the boundary of the open deposition hole and hydrostatic pressure is initially set in the model domain.

The resulting pressure field of phase 1 is used as the initial condition in the second phase. The hydraulic boundary conditions at the outer model boundaries are the same as in phase 1. At the upper and lower model boundaries, the hydrostatic pressure is applied as a boundary condition. At the symmetry axis, the outer vertical model boundary and the canister boundary, a 'no-flow' boundary condition is prescribed. For the mechanical calculations in stage 3 of the code comparison, the nodal displacements are fixed to zero at the symmetry axis, the canister boundary and the lower and the outer vertical boundary. A vertical load equal to the lithostatic stress at the corresponding depth is prescribed at the upper boundary. The temperature is initially set to 15°C in the model domain and fixed at the upper and lower model boundaries.

The evolution of the canister heat is simulated by applying an exponential expression (Equation 4) and assuming SKB's target initial power of 1700 W. The estimated values of the coefficients are given in Table 1. Closely spaced tabular values of the canister power evolution are provided as model input to avoid deviations in the results due to different ways of applying the heat source term.

$$P(t) = P(0)\sum_{i=1}^{7}\left[a_i \exp\left(-\frac{t}{t_i}\right)\right] \quad (4)$$

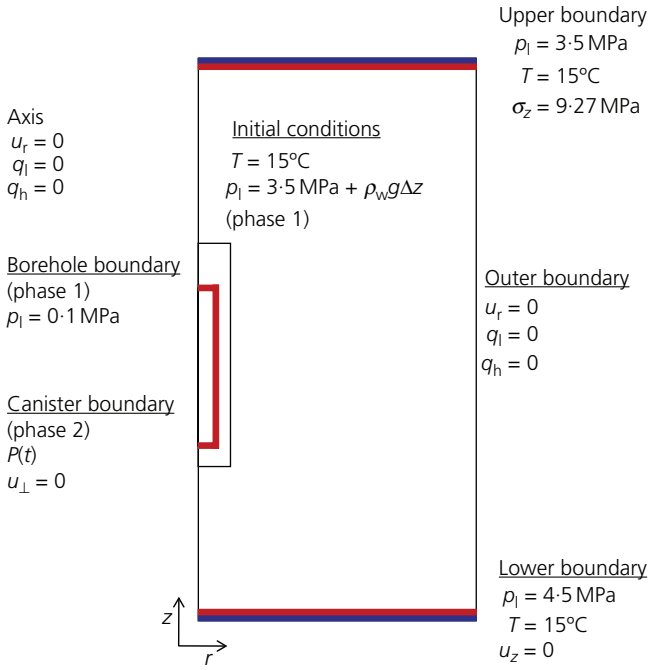

Figure 2. Boundary and initial conditions

Table 1. Time constants and coefficients for the exponential power expression

i	t_i: years	a_i
1	20	0·060147
2	50	0·705024
3	200	–0·054753
4	500	0·249767
5	2000	0·025407
6	5000	–0·009227
7	20 000	0·023877

with $P(0)$ as the canister power at time of deposition; a_i as the coefficients dependent on the fuel age; t as time; and t_i as time constants.

Material properties

To obtain a representative base case model for the sensitivity analysis, the material parameters were thoroughly defined based on literature data of experimental findings (Schäfers, 2011).

ROCK PROPERTIES

The sensitivity analysis is not site specific; therefore, a significant variability of the rock properties has been considered. Representative values for the rock properties were chosen for the benchmark model of the code comparison by either selecting parametric values from the literature or defining the values through parametric studies. The rock properties are compiled in Table 2.

The intrinsic permeability of the rock is set to $1 \times 10^{-17}\,\mathrm{m}^2$. It was determined in a parametric study to guarantee sufficient supply of water from the rock so that the saturation process of the EBS is controlled by the bentonite properties (Schäfers, 2011). The effects of rock fractures and the excavation-damaged zone are neglected.

The retention behaviour of the rock is described by a van Genuchten function (Equation 5) and the relative permeability k_{rel} by Equation 6. The corresponding parameters $P_{\mathrm{R},0}$ (in megapascals) and m_{R} are chosen based on measurement data from the Grimsel site (Finsterle and Pruess, 1995).

$$S_{\mathrm{l}}(s) = \left[1 + \left(\frac{s}{P_{\mathrm{R},0}}\right)^{1/(1-m_{\mathrm{R}})}\right]^{-m_{\mathrm{R}}} \quad (5)$$

$$k_{\mathrm{rel}}(S_{\mathrm{l}}) = \sqrt{S_{\mathrm{l}}}\left[1 - \left(1 - S_{\mathrm{l}}^{1/m_{\mathrm{R}}}\right)^{m_{\mathrm{R}}}\right]^2 \quad (6)$$

with S_{l} as the liquid saturation and s as the suction (in megapascals).

Calculations of the thermal conductivity from mineral analyses for different rock types at the Äspö site give values of 2·6 W/(m K) for Äspö diorite and 3·05 W/(m K) for Ävrö granite (Sundberg, 2003). The thermal state of the rock around the repository can be realistically modelled only at the repository scale. The spacing of the deposition holes and emplacement drifts as well as the rock mass surrounding the repository determine the temperature evolution in the near field, which cannot be adequately captured by a simplified 2D axisymmetric model. Since the benchmark model is on the deposition hole scale, the thermal conductivity is calibrated in a parametric study to reach representative maximum temperature values higher than 80°C in a point in the buffer close to the heater. The adopted parameter value for the benchmark model is 2·4 W/(m K) (Schäfers, 2011). The volumetric heat capacity was estimated from measurements to 2·16 MJ/(m^3 K) for Äspö diorite and 2·06 MJ/(m^3 K) for Ävrö granite, which are the main rock types at the Äspö site (Sundberg, 2003). With an assumed rock density of 2700 kg/m^3, this results in specific heat capacity values ranging from 760 to 800 J/(kg K). The adopted parameter value for the benchmark model is c = 770 J/(kg K); it was set to a fixed value for the calibration of the heat conductivity. The values for density, heat conductivity and heat capacity are used as solid-phase properties for the calculation of the porous medium properties.

Table 2. Parameters for rock material

Parameter	Symbol	Base case value	Source	Variations
Density	ρ_{R}	2700 kg/m^3	Åkesson *et al.* (2010a)	—
Porosity	n_{R}	0·003	Åkesson *et al.* (2010a)	0·001–0·005
Retention properties		Equation 5 $P_{\mathrm{R},0}$ = 1·74 MPa m_{R} = 0·60	Åkesson *et al.* (2010a), Finsterle and Pruess (1995)	$P_{\mathrm{R},0}$ = 5·50 MPa, m_{R} = 0·33 $P_{\mathrm{R},0}$ = 4·00 MPa, m_{R} = 0·65 $P_{\mathrm{R},0}$ = 0·70 MPa, m_{R} = 0·33
Intrinsic permeability	$k_{\mathrm{R,i}}$	$1·0 \times 10^{-17}$ m^2	Parametric study (Schäfers, 2011)	$1·0 \times 10^{-21}$–$1·0 \times 10^{-15}$ m^2
Relative permeability	$k_{\mathrm{R,rel}}$	Equation 6 m_{R} = 0·6	Åkesson *et al.* (2010a), Finsterle and Pruess (1995)	$k_{\mathrm{R,rel}} = S_{\mathrm{l}}^3$ $k_{\mathrm{R,rel}} = S_{\mathrm{l}}^{10}$
Tortuosity	τ_{R}	1·0	Åkesson (2006)	—
Heat conductivity	λ_{R}	2·4 W/(m K)	Parametric study (Schäfers, (2011)	2·4–3·9 W/(m K)
Specific heat capacity	c_{R}	770 J/(kg K)	Sundberg (2003)	750–850 J/(kg K)
Thermal expansion coefficient	$\alpha_{\mathrm{T,R}}$	$7·2 \times 10^{-6}$ K^{-1}	SKB (2006a)	—
Poisson's ratio	υ_{R}	0·24	Staub *et al.* (2002)	—
Young's modulus	E_{R}	62×10^3 MPa	Staub *et al.* (2002)	—

BUFFER PROPERTIES

The material parameters for the buffer are given in Table 3. The values for density and heat capacity are used as solid-phase properties.

A commonly applied suction–saturation relationship is the van Genuchten function. While this curve can be fitted nicely to suction values corresponding to saturations higher than the initial conditions, it displays larger deviations from the experimental data in the case of dehydration of the material (Åkesson *et al*., 2010a). The desaturation of the buffer due to the heating of the canister is an important aspect of the benchmark model. Therefore an extended van Genuchten function is applied (Equation 7), which can be adapted to the measured values for both increasing and decreasing saturation through fitting of the model parameters $P_{B,0}$ (in MPa) and m_B (Åkesson *et al*., 2010a).

$$S_l(s) = \left[1 + \left(\frac{s}{P_{B,0}}\right)^{1/(1-m_B)}\right]^{-m_B} \left(1 - \frac{s}{P_{B,1}}\right)^{m_{B,1}} \quad (7)$$

A general power law (Equation 8) is assumed for the relative permeability of bentonite buffer material (Börgesson and Hernelind, 1999).

$$k_{rel}(S_l) = S_l^{\delta} \quad (8)$$

A value of $\delta = 3$ is defined here, as determined by Börgesson and Hernelind (1999).

For those stages of the code comparison that consider two-phase flow, the relative permeability for the gas phase is given by Equation 9 based on assumptions by Åkesson (2006). As pointed out by Villar and Lloret (2001), the intrinsic permeability for gas flow in dry clay can differ by up to eight orders of magnitudes compared to water flow tests in saturated clay, which is attributed to differences in the microstructural arrangements due to the swelling of the clay.

$$k_{B,rel,g} = 1 \times 10^8 (1 - S_l)^4 \quad (9)$$

The heat conductivity of the buffer λ_B is described as a function of the degree of saturation. In the code comparison, the following expression is used (Åkesson *et al*., 2010a)

$$\lambda_B(S_l) = 0{\cdot}7(1 - S_l) + 1{\cdot}3S_l \quad (10)$$

Table 3. Parameters for buffer material

Parameter	Symbol	Base case value	Source	Variations
Particle density	ρ_B	2780 kg/m^3	Åkesson *et al*. (2010a)	—
Density at saturation	$\rho_{B,sat}$	2000 kg/m^3	Averaged based on the report by SKB (2010)	1950–2050 kg/m^3
Initial liquid saturation	$S_{l,0}$	0·61	Calculated based on the reports by Åkesson *et al*. (2010a), Börgesson *et al*. (2002) and SKB (2006b)	0·54–0·68
Porosity	n_B	0·438	Calculated based on the reports by Åkesson *et al*. (2010a), Börgesson *et al*. (2002) and SKB (2006b)	—
Retention properties	—	Equation 7 $P_{B,0}$ = 5·523 MPa m_B = 0·16 $P_{B,1}$ = 950 MPa $m_{B,1}$ = 1·6	Calculated based on the report by Åkesson *et al*. (2010a)	—
Intrinsic permeability	$k_{B,i}$	6·4 × 10^{-21} m^2	Calculated based on the reports by Åkesson *et al*. (2010a) and Börgesson *et al*. (1995)	3·8 × 10^{-21}–1·0 × 10^{-20} m^2
Relative permeability for the liquid phase	$k_{B,rel}$	S_l^3	Börgesson and Hernelind (1999)	S_l^2 S_l^4
Tortuosity	τ_B	1·0	Hökmark (2004)	0·1–1·0
Relative permeability for the gas phase (stage 2c)	$k_{B,rel,g}$	Equation 9	Åkesson (2006)	—
Heat conductivity	λ_B	Equation 10	Åkesson *et al*. (2010a)	Equation 11 Equation 12 Equation 13
Specific heat capacity (solid phase)	c_B	800 J/(kg K)	Börgesson and Hernelind (1999)	800–1100 J/(kg K)
Linear thermal expansion coefficient	$\alpha_{B,t}$	3·4 × 10^{-6} K^{-1}	Börgesson *et al*. (1995)	—
Poisson's ratio	ν_B	0·2	Åkesson *et al*. (2010a)	0·1–0·4
Young's modulus	E_B	20·0 MPa	Calculated based on the report by Åkesson *et al*. (2010b)	0·1–90·0 MPa
Maximum swelling pressure	$\sigma_{sw,\ max}$	13·4 MPa	Derived based on the report by Åkesson *et al*. (2010a), assuming linear dependence of swelling pressure on liquid saturation	5·6–29·7 MPa

Different expressions for the saturation-dependent heat conductivity are used in the sensitivity analysis (Åkesson *et al*., 2010a)

$$\lambda_B(S_l) = 0{\cdot}7(1 - S_l) + 1{\cdot}3S_l \quad (11)$$

$$\lambda_B(S_l) = 1{\cdot}3^{S_l^{0{\cdot}5}} \times 0{\cdot}33^{(1-S_l)^2} \quad (12)$$

$$\lambda_B(S_l) = 0{\cdot}5\cos^2\left(\frac{\pi S_l}{2}\right) + 1{\cdot}3\sin^2\left(\frac{\pi S_l}{2}\right) \quad (13)$$

The definition of the thermal expansion value for the buffer material is based on the findings of Börgesson *et al*. (1995). They concluded from thermal expansion tests performed on MX-80 samples that the thermo-mechanical interaction is dominated by the expansion of the pore water, not of the solid particles. The key parameters are the thermal expansion coefficient and the compressibility of pore water as well as the degree of saturation. The thermal expansion coefficient of the bentonite particles is therefore set to $3{\cdot}4 \times 10^{-6}\,K^{-1}$, and it is not varied in the sensitivity analysis.

Assuming a linear dependence of the swelling pressure on liquid saturation, the maximum swelling pressure $\sigma_{sw,max} = 13{\cdot}4$ MPa is derived from the initial liquid saturation and density at saturation according to the report by Åkesson *et al*. (2010a).

FLUID PROPERTIES

The fluid properties are listed in Table 4. To simplify the numerical model, the fluid viscosity and density are kept constant in stages 1, 2a, 2c, 3a and 3b of the code comparison. Since the temperature dependence of the fluid properties has a significant influence on the modelling results, stage 2b – where temperature-dependent fluid properties were considered – was added to the code comparison. The temperature-dependent fluid density was given as tabulated values, based on the publication by Bettin and Spieweck (1990). The values for the fluid viscosity are derived by Equation 14 (Yaws *et al*., 1976) and were given as tabulated values.

$$\mu(T) = 1 \times 10^{-3} \exp\left(-24{\cdot}711 + 4209{\cdot}1/T + 0{\cdot}04527T - 3{\cdot}376 \times 10^{-5}T^2\right) \quad (14)$$

with μ as the viscosity in pascal-seconds and T as the temperature in kelvin.

Sensitivity analysis

Variation of material properties

One major goal of the sensitivity analyses is to study the effects of parameter variations on the modelling results and to identify the key parameters of the numerical model. The considered variations of material parameters are given in Tables 2 and 3. They include the rock and buffer properties relevant for the thermal, hydraulic and mechanical processes. As a first approach to assessing the influence of individual parameters on the output quantities with reasonable computational costs, it was decided to conduct a local sensitivity analysis – that is, to vary one parameter at a time. This first analysis will lead to an understanding of the influence of single parameters on the modelling results and may serve as the basis for more computational demanding analyses varying multiple parameters at a time.

An exception is the variation of the initial state of the buffer. As specified in the design premises for the KBS-3 concept, the density at saturation for MX-80 bentonite ranges between 1950 and 2050 kg/m^3 (SKB, 2010). An average value of 2000 kg/m^3 is assumed in the base case model. In the sensitivity analysis, the minimum and maximum values of the bentonite density at saturation are investigated, including the variation of initial liquid saturation, porosity, retention properties, intrinsic permeability, Young's modulus and maximum swelling pressure.

Variations of boundary and initial conditions

Model uncertainties concern not only the material parameters, but also the applied boundary and initial conditions.

To derive the initial hydraulic state in the rock before the emplacement of the canister, a purely hydraulic calculation of the open deposition hole is conducted. In the base case, a relative humidity of 100% and a water pressure of 0·1 MPa are assumed at the borehole boundaries. Variations considered in the sensitivity analysis include applying a lower relative humidity (80%) to the borehole boundary, omitting and extending this first calculation phase (from 30 d to 30 years).

SKB's target initial power of 1700 W is applied to the base case model. Different initial power assumptions are considered, from 1837 W for 30-year-old fuel to 1545 W for 40-year-old fuel based on the report by Hökmark and Fälth (2003). The corresponding canister power evolutions are depicted in Figure 3.

Table 4. Liquid phase input parameters

Parameter	Symbol	Value	Source
Density	ρ_l	1000 kg/m^3 or $\rho_l = f(T)$ (stage 2b)	Approximation (Bettin and Spieweck, 1990)
Viscosity	μ_l	$1{\cdot}0 \times 10^{-3}$ Pa s or Equation 14 (stage 2b)	Approximation (Yaws *et al*., 1976)
Heat conductivity	λ_l	0·6 W/(m K)	Approximation (Ramires *et al*., 1994)
Specific heat capacity	c_l	4·183 kJ/(kg K)	Approximation (Wagner and Pruß, 2002)

Variations of considered physical processes

Neglecting different physical processes and their coupling relations in the numerical model may help identify those processes which dominate the coupled system behaviour. Furthermore, the variation of considered processes is of particular interest when comparing different numerical tools. It may help identify potential influences of different implementations of physical processes on the modelling results. Variations considered in the sensitivity analysis include the neglect of thermal and mechanical processes as well as omitting vapour diffusion and considering temperature-dependent fluid properties, adding or omitting one process at a time.

Code comparison

Stages of the code comparison

The code comparison was divided into six different stages with increasing complexity of the coupled simulation. Temperature effects from the heating of the canister are considered in all stages of the code comparison. In stage 1, vapour diffusion is neglected and the fluid flow is simulated using Richards's approximation. In stage 2a, the simulation is extended by including vapour diffusion. To account for the effects of temperature changes on the fluid properties, the fluid density and viscosity are defined as functions of the temperature in stage 2b. In stage 2c, a two-phase flow simulation is performed, taking into account the changes in gas phase pressure. In the THM simulations of stages 3a and 3b, Richards's approximation is applied, vapour diffusion is considered and the temperature-dependent fluid properties are neglected. For the mechanical process, only the elastic material behaviour is considered in stage 3a, neglecting the swelling term in Equation 1. In stage 3b, a term for the swelling of the bentonite is considered by the simplified swelling law (Equation 1).

Codes and models

TOUGH2 AND FLAC3D USED BY WOOD

The numerical modelling performed by Wood is achieved through the coupling of Tough2 and Flac3D. Tough–Flac3D coupling was presented as a pragmatic approach for modelling coupled multiphase flow, heat transport and geomechanical problems (Rutqvist and Tsang, 2003). In this approach, Tough2, an integral finite-difference code, is used for solving multiphase flow and heat transport equations, whereas Flac3D, a finite-volume code, is used for solving geomechanical stress–strain equations through a sequential coupling. For the purposes of this modelling task, only a unidirectional coupling between the hydraulic and the mechanical process is assumed, neglecting the effects of the mechanical behaviour on the hydraulic-thermal processes. The EOS7R module of Tough2 was utilised for the modelling of all stages. To achieve a Richards-type approximation (requirement of stage 1) using EOS7R, the following assumptions were introduced: assignment of high gas permeability in the buffer (five orders of magnitude higher than the liquid permeability) and the host rock (two orders of magnitude higher than the liquid permeability) and introduction of an outflow boundary condition only for the gas phase on the canister buffer interface, allowing the gas to 'disappear' through the canister wall. For the mechanical processes in the bentonite, the swelling law proposed in the task description (Equation 2) is applied.

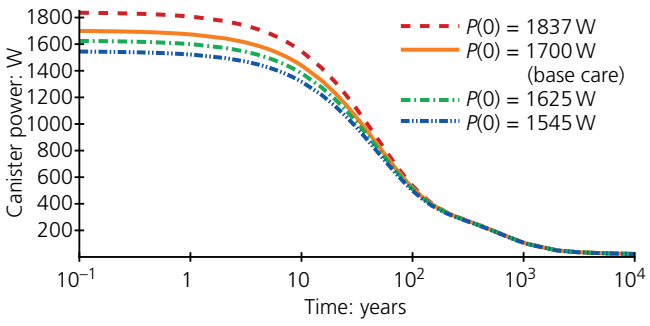

Figure 3. Variations of canister power evolution

OGS USED BY BGR

BGR uses the finite-element (FE) code OGS, which proved suitable for modelling the behaviour of clay-rich materials as engineered barriers (Nowak, 2007; Nowak and Kunz, 2010). The governing equations of coupled THM problems can be found in the papers by Wang *et al*. (2009, 2010). In OGS, Richards's approximation is available, as well as non-isothermal two-phase flow. For the mechanical processes in the bentonite, a simplified swelling law is applied, as proposed in the task description (Equation 2). While full coupling between the hydraulic and mechanical process is implemented in OGS, for this task only unidirectional coupling is considered between the hydraulic and mechanical processes. While the saturation and pore pressure influence the stress components, the effect of the mechanical behaviour on the hydraulic process is neglected.

LOSTUF USED BY CRIEPI

Criepi developed an in-house coupled THM analysis program, Lostuf (Sawada *et al*., 2017). The original formulation of coupled hydroelasticity was extended to a partially saturated thermo-hydroelastic medium; the hydraulic processes are based on Richards's approximation. For the models used in the code comparison, the effect of the mechanical behaviour on the hydraulic process is neglected and the mechanical behaviour of the bentonite is described by an elastic constitutive equation. The swelling pressure is defined in linear dependence on the liquid saturation, as proposed in the task description (Equation 2).

LAGAMINE USED BY EPFL

The modelling activity carried out at EPFL used the FE environment Lagamine (Charlier, 1987; Charlier *et al*., 2001). The code was developed by the Department of Geomechanics and Engineering Geology of the University of Liège. The Soil Mechanics Laboratory of EPFL contributed in the development and implementation of constitutive laws for partially saturated soils under non-isothermal conditions. Lagamine uses a compositional approach to write the mass balance equations, meaning that the mass balances are described for the species rather than for the phases. The liquid phase contains two species, liquid water and

dissolved air, while the gas phase is composed of dry air and water vapour. The equilibrium between liquid water and water vapour is controlled by the temperature. The solid, liquid and water phases are assumed in thermal equilibrium, and a unique temperature is defined for the whole mixture. Heat transport is governed by conduction and convection, with the thermal conductivity of the mixture obtained as a volume-weighted average of the thermal conductivity of each phase. A more detailed description of the use of Lagamine by EPFL for the reported modelling activity can be found in the paper by Qiao *et al*. (2015).

COMSOL MULTIPHYSICS USED BY CLAY TECHNOLOGY

The numerical modelling done at Clay Technology was carried out using Comsol Multiphysics (Comsol, 2017). While most of the physics required for the code validation task was readily available as part of the main program and modules (subsurface flow, structural mechanics), some parts were not. In particular, vapour diffusion had to be implemented using the weak contribution interface following a similar formulation to that used in Code_Bright (see later). In stage 3b of the code comparison, the swelling term is added as a strain contribution in the linear elastic interface. This was accomplished by modifying the built-in hygroscopic strain contribution ε_{hs} so that the term

$$\varepsilon_{hs} = \frac{\sigma_{sw,max} S_l}{E(1-2\upsilon)} \quad (15)$$

was added to the inelastic strain.

CODE_BRIGHT USED BY UPC

UPC uses Code_Bright, an FE code that enables coupled THM analysis in geological media. The mechanical models used are a linear elastic one for the rock in all models and for the bentonite in the most basic case. In the case of swelling of the bentonite being taken into account, a thermo-elasto-plastic model is considered, in which the volumetric deformation depends on the suction and mean effective stress; the specified relationship between the degree of saturation and the swelling stress is not available in the code. Also, the bidirectional hydro-mechanical coupling cannot be switched off in Code_Bright. Instead, a model is used that shows the most similarities to the specified swelling model. More information about these models can be found in the *Code_Bright User's Guide* (UPC, 2017). In the Code_Bright model for stage 3b of the code comparison, the two-directional coupling between the hydraulic and mechanical process is taken into account – that is, the porosity of the bentonite is changed by the swelling process.

SPATIAL DISCRETISATION

In the base case development for the sensitivity analysis, the influence of the spatial discretisation on the model accuracy was evaluated (Schäfers, 2011). This emphasised the importance of a mesh convergence study before conducting the code comparison. The number of elements between the observation points and the buffer–rock interface proved to be a decisive parameter. Characteristic values of the spatial discretisation of the different models used in the code comparison are summarised in Table 5.

Results

The modelling results are presented as time plots for different points in the buffer. The evolution of the output quantities temperature T, pore water pressure p_l and suction s, liquid saturation S_l and the stress components σ_{rad}, σ_{tan} and σ_{axi} are compared for three points in the upper buffer section (P01–P03) and three points in the mid-heater section (P11–P13) (Figure 4).

Each calculation case is characterised by a set of input variables X_i – the so-called independent variables – and a set of output variables Y (X_i) – or dependent variables. The following seven output variables Y (X_i) are determined for the six observation points

- value and time of maximum temperature – T_{max}, $t(T_{max})$
- time of full liquid saturation – $t(S_l > 0{\cdot}99)$
- value of maximum suction – s_{max}
- values of stress components after 1000 years – σ_{rad}, σ_{tan} and σ_{axi}.

To facilitate the comparison between the different calculation cases, the absolute change in the dependent variable relative to the base case value is calculated (Equation 16).

$$\left|\frac{\Delta Y}{Y_0}\right| = \left|\frac{Y(X_i) - Y(X_0)}{Y(X_0)}\right| \quad (16)$$

To quantify the influence that a change in the input variable has on the output quantities, a relative change in the dependent variable by more than 10% is assumed to represent a 'high' influence, while a

Table 5. Characteristic values of model spatial discretisation used in the code comparison

Code	Mesh		
	Element type	Number of elements	Number of elements across mid-heater section
Tough2–Flac3D	Quad	4156	14
OGS	Tri	14 871	16
Lostuf	Quad	16 000	16
Lagamine	Quad	2768	10
Comsol	Quad-Tet mix	5836	8
Code_Bright	Quad	3206 or 3964 (stage 3)	12 or 14 (stage 3)

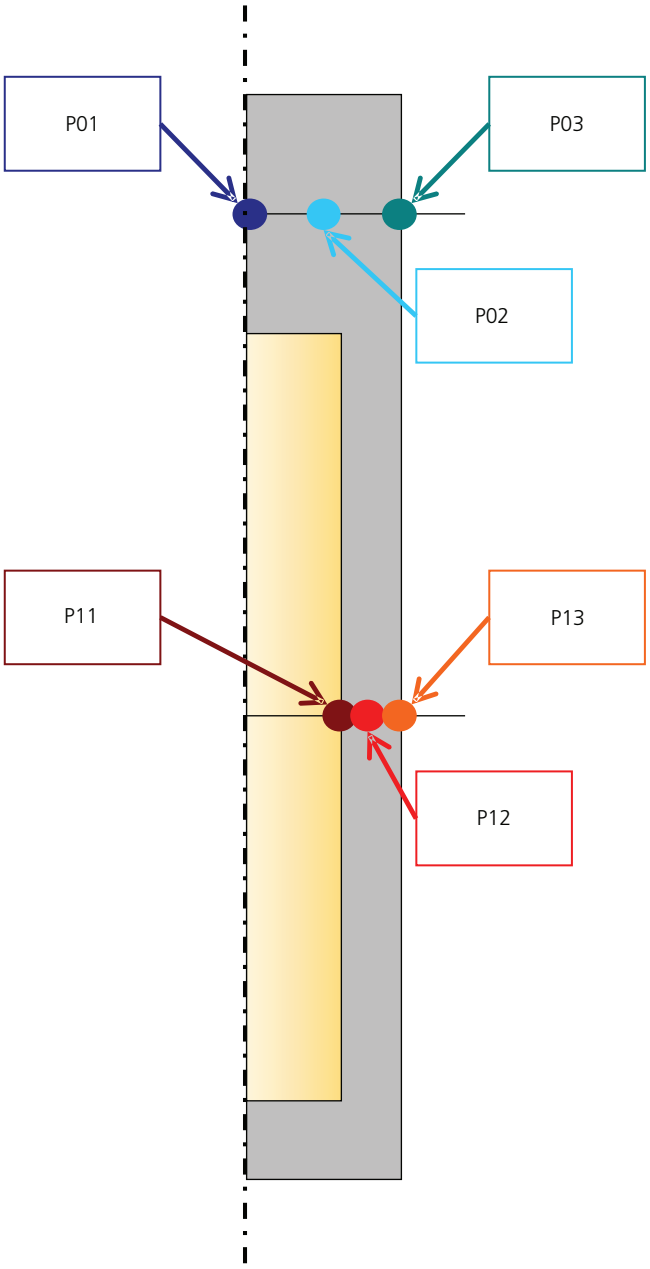

Figure 4. Location of observation points

relative change below 10% is assumed to represent a 'low' degree of influence of the parameters for the selected ranges.

Results of the sensitivity analysis

The sensitivity analysis was performed by different teams using different numerical codes (Gordon *et al.*, 2014; Sawada, 2016; Schäfers, 2012).

Variations of material properties

Exemplary results of calculations performed by BGR using the FE code OGS are shown in Figures 5 and 6. An increase in the heat conductivity of the rock from 2·4 to 3·9 W/(m K) leads to a decrease in temperatures in all observation points in the buffer (Figure 5). The maximum temperature at point P11 is reduced from 81 to 65°C, a relative change of approximately 20%.

Changing the buffer intrinsic permeability results in changes in the evolution of liquid saturation in the buffer (Figure 6). The time until full liquid saturation ($S_l > 0{\cdot}99$) is reached at point P01 varies between 4·1 years for $k_{B,i} = 1{\cdot}0 \times 10^{-20}$ m^2 and 8·5 years for $3{\cdot}8 \times 10^{-21}$ m^2. Related to the base case result of 5·8 years, this represents a relative change of approximately 29–46%.

Based on the relative change in output quantities (Equation 16), the degree of influence of each input variable variation on the thermal, hydraulic and mechanical process is identified (Table 6). The material parameters that are identified to have a significant influence on one or more output quantities are: rock intrinsic permeability, buffer intrinsic permeability, buffer density at saturation (including retention, permeability and swelling pressure), rock thermal conductivity, buffer tortuosity and rock retention. While some parameters show an influence on the evolution of the stress components in the buffer, only the

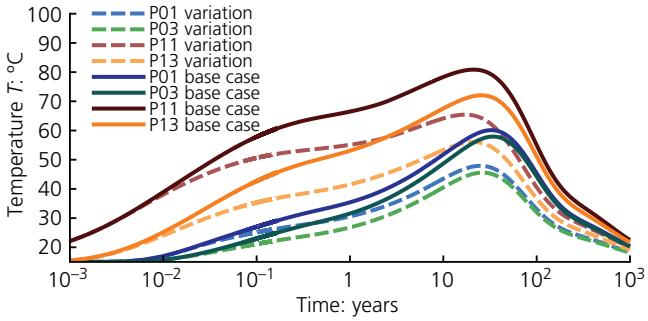

Figure 5. Range of temperature evolution at different points in the buffer for variation of heat conductivity of the rock ('base case': 2·4 W/(m K); 'variation': 3·9 W/(m K)) – results of OGS calculations

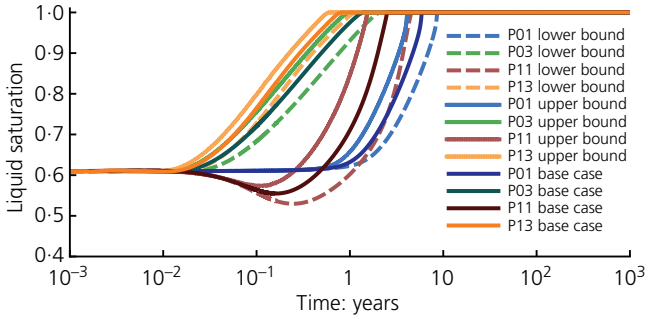

Figure 6. Range of liquid saturation evolution at different points in the buffer for variation of buffer intrinsic permeability ('lower bound': $3{\cdot}8 \times 10^{-21}$ m^2; 'upper bound': $1{\cdot}0 \times 10^{-20}$ m^2) – results of OGS calculations

variation of the initial density of saturation (including the initial saturation and maximum swelling pressure) has a significant influence on the final value of stress in the buffer.

Variations of boundary and initial conditions

The results of the variation of boundary and initial conditions show that the variation of the initial canister power within the defined range has a moderate influence on the calculated temperatures in the buffer. In the OGS results, the maximum temperature at point P11 shows an absolute variation of approximately 10°C for a variation in initial canister power between 1545 and 1837 W (Figure 7).

Considering a desaturation of the rock in the near field of the borehole before deposition also influences the modelling results. The thermal as well as the hydraulic output quantities change by more than 10% relative to the base case results when considering desaturation.

Variations of considered physical processes

The calculations performed by Criepi using the code Lostuf included the coupling between mechanical and hydraulic processes. The variation of considered processes showed that this coupling has a significant influence on the results.

In the base case of the sensitivity analysis, the fluid viscosity is defined as a function of temperature (Equation 14). Neglecting this temperature dependence has the effect that the calculated time until full liquid saturation is reached in the buffer is extended significantly (Figure 8) – at point P11 from 2·5 years in the base case to 5·6 years in the case with a constant fluid viscosity. The

Table 6. Identified degree of influence of material parameter variations within the selected ranges on selected output quantities – calculations using the FE code OGS

Parameter	Degree of influence on output quantities: %		
	Thermal	Hydraulic	Mechanical
Rock intrinsic permeability	**20**	**>100**	2
Buffer intrinsic permeability	<1	**46**	<1
Buffer density at saturation (including retention, permeability and swelling pressure)	<1	**24**	**90**
Rock thermal conductivity	**12**	**21**	<1
Buffer tortuosity	<1	**18**	<1
Rock retention properties	<1	**15**	<1
Rock porosity	<1	8	<1
Buffer thermal conductivity	<1	8	<1
Rock relative permeability	<1	5	<1
Rock thermal capacity	2	2	<1
Buffer relative permeability	<1	<1	<1
Buffer thermal capacity	<1	<1	<1
Buffer Poisson's ratio	<1	<1	<1
Buffer Young's modulus	<1	<1	<1

Bold numbers indicate that the influence corresponds to a relative change of more than 10%

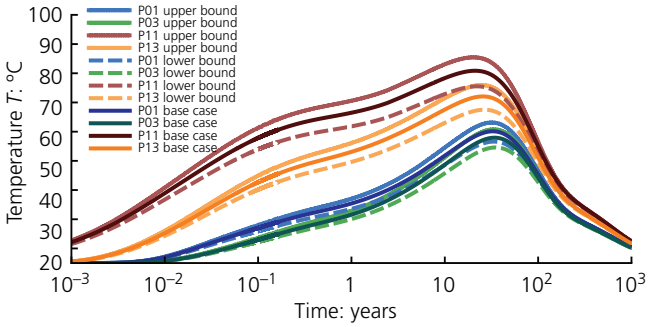

Figure 7. Range of temperature evolution at different points in the buffer for variation of initial canister power ('lower bound': 1545 W; 'upper bound': 1837 W) – results of OGS calculations

temperature in the buffer reaches values of about 80°C, which causes the temperature-dependent viscosity in the base case to decrease to values of approximately $3{\cdot}2 \times 10^{-4}$ Pa s. The viscosity in the case with constant fluid properties is thus with a constant value of $1{\cdot}0 \times 10^{-3}$ Pa s overestimated through large parts of the simulation. According to Darcy's equation, the fluid velocity is inversely proportional to the fluid viscosity. An overestimation of the viscosity leads to a slowing down of the fluid velocity compared to the base case, which is the reason for the extended time until full liquid saturation.

Results of the code comparison

In the following sections, selected results of the code comparison are described.

TH calculation considering vapour diffusion and temperature-dependent fluid properties

In general, the thermal and hydraulic results showed very good agreement between all codes in all stages of the code validation. As an example, the results from stage 2b, where Richards's approximation is applied and vapour diffusion as well as temperature-dependent fluid properties (i.e. fluid density and

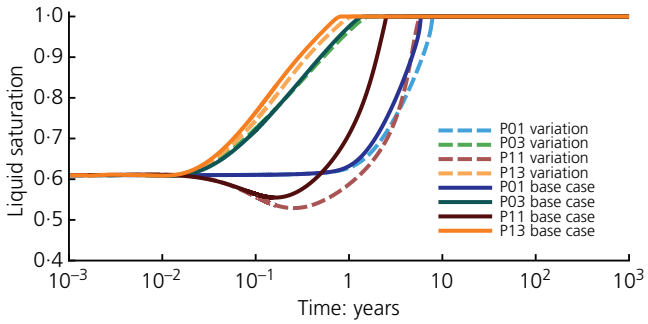

Figure 8. Change in liquid saturation evolution at different points in the buffer for variation of considered physical processes ('variation': neglecting temperature-dependent fluid viscosity) – results of OGS calculations

viscosity) are considered, are described in the following sections. All six teams participated in this stage.

THERMAL RESULTS

In Figure 9, the calculated temperature profiles for one point in the buffer in stage 2b are compared. The value of the maximum temperature at the point closest to the heater (P11) varies between 81°C (OGS, Lagamine, Comsol) and 82°C (Lostuf, Code_Bright), while the time that the maximum is reached lies between 19·7 years (Code_Bright) and 21·5 years (Tough2). The calculated temperature evolutions agree very well for all points in the buffer. The small deviations between the results of the different codes (below 1°C and 1·8 years, respectively, at point P11) can be attributed to differences in the partitioning of calculation and evaluation time steps – in the case where too few evaluation time steps are used, the time when the peak temperature is reached and the evaluation time steps may not coincide. The relative deviation in the calculated temperature maxima for all observation points is below 2%.

HYDRAULIC RESULTS

The hydraulic processes are evaluated using liquid saturation and liquid pressure at different points of the buffer. Examples are shown in Figures 10 and 11. At the point closest to the heater, full liquid saturation is reached after 2·2 years (Tough2) to 2·8 years (Lagamine). The differences of the results of the Tough2 calculation compared to those of the other codes can be attributed to the fact that, instead of Richards's approximation, a mobile gas model is applied in Tough2. Overall, the qualitative and quantitative agreement between the results of the different codes is very good.

THM calculation with a simplified swelling term for the bentonite

THERMAL RESULTS

Since the coupling between thermal and mechanical processes is considered unidirectional (in the form of temperature-induced stresses), the temperature evolution calculated in stage 3b is similar to that in stages 2a, 2b and 2c (stage 2b results are illustrated in Figure 9). As the case in those stages, the results of the different codes agree very well in terms of the qualitative and quantitative temperature evolution at different points in the buffer.

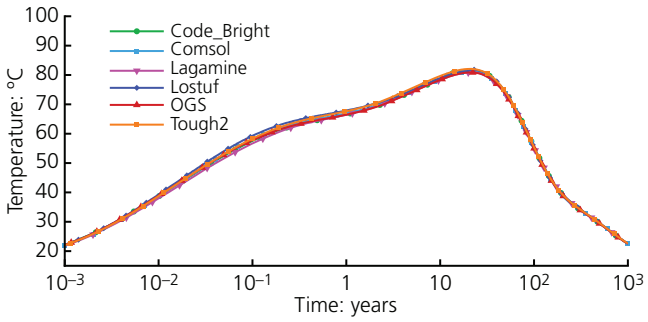

Figure 9. Stage 2b – temperature evolution at point P11

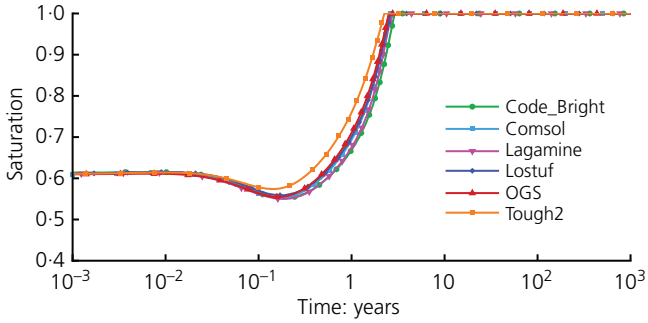

Figure 10. Stage 2b – evolution of liquid saturation at point P11

HYDRAULIC RESULTS

In Figure 11, the evolution of liquid saturation at point P11 is shown. As in stage 2, the saturation decreases at early times due to the strong temperature increase close to the heater. The time that full liquid saturation is reached at point P11 varies between 4·9 years (Tough2) and 6·4 years (Code_Bright). Some differences in the liquid saturation profiles can be observed, particularly between the results of Code_Bright and those of the other codes. This deviation can be attributed to the different coupling mechanisms between hydraulic and mechanical processes as well as to the different swelling models. The Code_Bright model considers the change of porosity due to the swelling of the bentonite. Therefore, when porosity diminishes, both liquid saturation degree and liquid pressure tend to increase, since there is less space for the embedded water. The other models do not consider this coupling, as defined in the task description.

MECHANICAL RESULTS

An example of the mechanical results from stage 3b can be found in Figure 12, where the time evolution of the effective radial stresses at point P11 is shown. As the liquid saturation increases due to the inflow from the rock, swelling pressure is induced in the buffer. Once full liquid saturation is reached at the point (after approximately 6 years for point P11), the liquid pressure contributes to the effective stress according to Equation 2, which leads to a sudden decrease in the compressive stress. After 10

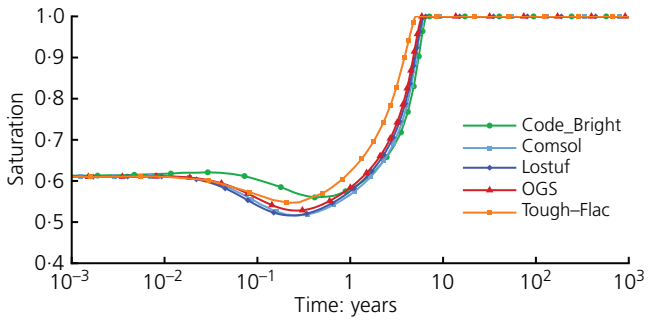

Figure 11. Stage 3b – evolution of liquid saturation at point P11

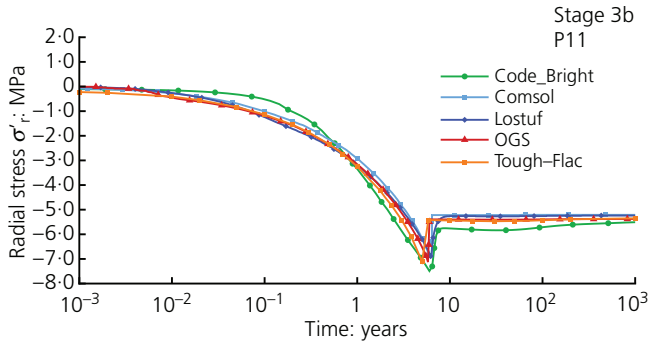

Figure 12. Stage 3b – evolution of radial stress at point P11

years, the effective radial stress reaches a value of approximately 5 MPa. Some deviations occur between the Code_Bright results and the results of the other codes, which can be attributed to the differences in the saturation evolution and different swelling models. Overall, the mechanical results agree qualitatively and quantitatively for all codes.

Conclusions

The sensitivity analysis performed as one of the tasks within the Task Force on Engineered Barrier Systems included variations of material parameter values, boundary and initial conditions, considered physical processes and alternative model geometries, amounting to 60 different modelling cases. This in-depth analysis helped evaluate the influence of parameter and conceptual uncertainties on the results of coupled THM modelling of EBS and identify key parameters and key processes. Among these parameters, which proved to have a significant influence on the thermal, hydraulic or mechanical output quantities, are the rock intrinsic permeability, the buffer density at saturation (including maximum swelling pressure, intrinsic permeability and retention behaviour), rock thermal conductivity and rock retention properties. Furthermore, it was demonstrated that the consideration of the mechanical–hydraulic coupling strongly affects the saturation evolution in the buffer. An in-depth knowledge of the parameters and processes affecting the modelling results will be valuable also for future modelling activities within the Task Force on Engineered Barrier Systems and elsewhere.

From the code comparison, it can be concluded that very good agreement between the results of the different codes was achieved for the coupled TH processes, taking into account Richards's approximation, vapour diffusion and temperature-dependent fluid properties. For the coupled THM processes, some deviations remain, while the overall qualitative agreement is good. For the remaining differences, explanations were identified, among these are differences in process couplings and definition of the mechanical material behaviour of the bentonite.

One crucial aspect, which is well known to numerical modellers but which should be pointed out once again, is the importance of discretisation studies prior to running the actual simulations. In the code comparison, it was shown that the number of elements between the observation points and the material interfaces is decisive for the time until liquid saturation is reached, but the temporal discretisation and the number of evaluation steps were also shown to influence the agreement of the results.

The cross-code comparison encouraged a fruitful exchange among modelling teams. In particular, the stepwise increase in the complexity of the coupled simulation helped provide in-depth insights into the individual behaviour of the codes when modelling the coupled THM behaviour of the EBS. Serving as a benchmark example for coupled THM simulations of bentonite-based EBS, the code comparison task will support comparisons between modelling results and experimental data, which are performed within the Task Force on Engineered Barrier Systems. This can contribute to increase the confidence in the modelling capabilities of several codes used for safety evaluations of repositories for spent fuel and high-level radioactive waste.

Acknowledgements

The authors would like to thank the Task Force on Engineered Barrier Systems project team for the fruitful co-operation. Parts of the presented work were financially supported by the German Federal Ministry for Economic Affairs and Energy, as well as the Swiss National Cooperative for the Disposal of Radioactive Waste, the Radioactive Waste Management Ltd and the Swedish Nuclear Fuel and Waste Management Company.

REFERENCES

Åkesson M (ed.) (2006) *Äspö Hard Rock Laboratory – Temperature Buffer Test – Evaluation Modeling – Field Test*. SKB, Stockholm, Sweden, SKB IPR-06-10.

Åkesson M, Börgesson L and Kristensson O (2010a) *SR-site Data Report: THM-modelling of Buffer, Backfill and Other System Components*. SKB, Stockholm, Sweden, SKB TR-10-44.

Åkesson M, Kristensson O, Börgesson L, Dueck A and Hernelind J (2010b) *THM Modelling of Buffer, Backfill and Other System Components: Critical Processes and Scenarios*. SKB, Stockholm, Sweden, SKB TR-10-11.

Bettin H and Spieweck F (1990) *Die Dichte des Wassers als Funktion der Temperatur nach Einführung der Internationalen Temperaturskala von 1990*. Physikalisch-Technische Bundesanstalt, Brunswick, Germany. PTB-Mitteilungen 100(1990)3 (in German).

Börgesson L and Hernelind J (1999) *Coupled Thermo-hydro-mechanical Calculations of the Water Saturation Phase of a KBS-3 Deposition Hole: Influence of Hydraulic Rock Properties on the Water Saturation Phase*. SKB, Stockholm, Sweden, SKB TR-99-41.

Börgesson L, Johanesson LE, Sandén T and Hernelind J (1995) *Modelling of the Physical Behaviour of Water Saturated Clay Barriers: Laboratory Tests, Material Models and Finite Element Application*. SKB, Stockholm, Sweden, SKB TR-95-20.

Börgesson L, Gunnarsson D, Johanesson LE and Sandén T (2002) *Äspö Hard Rock Laboratory: Prototype Repository – Installation of Buffer, Canisters, Backfill and Instruments in Section 1*. SKB, Stockholm, Sweden, SKB IPR-02-23.

Charlier R (1987) *Approche unifiée de quelques problèmes non linéaires de mécanique des milieux continus par la méthode des éléments finis (grandes déformations des métaux et des sols, contact unilatéral de solides, conduction thermique et écoulements en milieu poreux)*. PhD thesis, Université de Liège, Liège, Belgium (in French).

Charlier R, Radu JP and Collin F (2001) Numerical modelling of coupled transient phenomena. *Revue Française de Génie Civil* **5(6)**: 719–741, https://doi.org/10.1080/12795119.2001.9692324.

Comsol (2017) *COMSOL Multiphysics Reference Manual, Version 5.3*. Comsol AB, Stockholm, Sweden. See http://www.comsol.com (accessed 29/12/2017).

Finsterle S and Pruess K (1995) Solving the estimation–identification problem in two-phase flow modeling. *Water Resources Research* **31(4)**: 913–924, https://doi.org/10.1029/94WR03038.

Gens A, Garcia-Molina AJ, Olivella S, Alonso EE and Huertas F (1998) Analysis of a full scale in situ test simulating repository conditions. *International Journal for Numerical and Analytical Methods in Geomechanics* **22(7)**: 515–548, https://doi.org/10.1002/(SICI)1096-9853(199807)22:7<515::AID-NAG926>3.0.CO;2-8.

Gordon A, Hoch A, Holton D and Baxter S (2014) *Sensitivity Analysis: Verification and Sensitivity Cases*. Amec, Harwell Oxford, UK, 03453-AG-0001/SV012013/14.

Hökmark H (2004) Hydration of the bentonite buffer in a KBS-3 repository. *Applied Clay Science* **26(1–4)**: 219–233, https://doi.org/10.1016/j.clay.2003.12.034.

Hökmark H and Fälth B (2003) *Thermal Dimensioning of the Deep Repository: Influence of Canister Spacing, Canister Power, Rock Thermal Properties and Nearfield Design on the Maximum Canister Surface Temperature*. SKB, Stockholm, Sweden, SKB TR-03-09.

Nowak T (2007) *Äspö Hard Rock Laboratory: Äspö Task Force Engineered Barrier System – Modelling of THM-coupled Processes for Task 1, Benchmarks 1, Using GeoSys/Rock Flow*. SKB, Stockholm, Sweden, SKB IPR-07-13.

Nowak T and Kunz H (2010) *Äspö Hard Rock Laboratory: Äspö Task Force on Engineered Barrier System – Modelling of THM-coupled Processes for Benchmark 2.2 with the Code GeoSys/RockFlow*. SKB, Stockholm, Sweden, SKB IPR-10-07.

Qiao YF, Ferrari A, Laloui L and Ding WQ (2015) Sensitive THM coupled analysis of buffer–rock barriers for nuclear waste storage. *Proceedings of the 7th Asian-Pacific Conference on Unsaturated Soils, Guilin, China*, pp. 665–670.

Ramires MLV, Nieto de Castro CA, Nagasaka Y *et al.* (1994) Standard reference data for the thermal conductivity of water. *Journal of Physical and Chemical Reference Data* **24(3)**: 1377–1381, https://doi.org/10.1063/1.555963.

Rutqvist J and Tsang CF (2003) TOUGH-FLAC: a numerical simulator for analysis of coupled thermal-hydrologic-mechanical processes in fractures and porous geological media under multi-phase flow conditions. *Proceedings of the TOUGH Symposium, Berkeley, CA, USA*, pp. 12–14.

Rutqvist J and Tsang CF (2008) *Review of SKB's Work on Coupled THM Processes within SR-Can*. Swedish Nuclear Power Inspectorate, Stockholm, Sweden, SKI Report 2008:08.

Sawada M (2016) *Sensitivity Analysis – Final Report*. Central Research Institute of Electric Power Industry, Abiko, Japan.

Sawada M, Nishimoto S and Okada T (2017) New rapid evaluation for long-term behavior in deep geological repository by geotechnical centrifuge – part 2 numerical simulation of model tests in isothermal condition. *Rock Mechanics and Rock Engineering* **50(1)**: 159–169, https://doi.org/10.1007/s00603-016-1061-6.

Schäfers A (2011) *Task Force on Engineered Barrier Systems: Sensitivity Analysis – Base Case Development – Annual Report 2010*. Bundesanstalt für Geowissenschaften und Rohstoffe, Hanover, Germany.

Schäfers A (2012) *Task Force on Engineered Barrier Systems: Sensitivity Analysis – Results of BGR's calculations I – Annual Report 2012*. Bundesanstalt für Geowissenschaften und Rohstoffe, Hanover, Germany.

SKB (Swedish Nuclear Fuel and Waste Management Company) (2006a) *Preliminary Site Description. Laxemar Subarea – Version 1.2*. SKB, Stockholm, Sweden, SKB R-06-10.

SKB (2006b) *Long-term Safety for KBS-3 Repositories at Forsmark and Laxemar – a First Evaluation: Main Report of the SR-Can Project*. SKB, Stockholm, Sweden, SKB TR-06-09.

SKB (2010) *Design, Production and Initial State of the Buffer*. SKB, Stockholm, Sweden, SKB TR-10-15.

Staub I, Fredriksson A and Outters N (2002) *Strategy for a Rock Mechanics Site Descriptive Model: Development and Testing of the Theoretical Approach*. SKB, Stockholm, Sweden, SKB R-02-02.

Sundberg J (2003) *Thermal Properties at Äspö HRL: Analysis of Distribution and Scale Factors*. SKB, Stockholm, Sweden, SKB R-03-17.

UPC (Universitat Politècnica de Catalunya) (2017) *Code_Bright User's Guide: Version 7.4, November 2017*. Departament d'Enginyeria del Terreny, Cartogràfica i Geofísica, UPC, Barcelona, Spain.

Villar MV and Lloret A (2001) Variation of the intrinsic permeability of expansive clays upon saturation. In *Clay Science for Engineering* (Adachi K and Fukue M (eds)). Balkema, Rotterdam, the Netherlands, pp. 259–266.

Wagner W and Pruß A (2002) The IAPWS Formulation 1995 for the Thermodynamic Properties of Ordinary Water Substance for General and Scientific Use. *Journal of Physical and Chemical Reference Data* **31(2)**: 387–535, https://doi.org/10.1063/1.1461829.

Wang W, Kosakowski G and Kolditz O (2009) A parallel finite element scheme for thermo-hydro-mechanical (THM) coupled problems in porous media. *Computers & Geosciences* **35(8)**: 1631–1641, https://doi.org/10.1016/j.cageo.2008.07.007.

Wang W, Rutqvist J, Görke UJ, Birkholzer JT and Kolditz O (2010) Non-isothermal flow in low permeable porous media: a comparison of Richard's and two-phase flow approaches. *Environmental Earth Sciences* **62(6)**: 1197–1207, https://doi.org/10.1007/s12665-010-0608-1.

Yaws CL, Miller JW, Shah PN, Schorr GR and Patel PM (1976) Correlation constants for chemical compound. *Chemical Engineering* **83(25)**: 153–162.